Drug-induced increase in lysobisphosphatidic acid reduces the cholesterol overload in Niemann-Pick type C cells and mice

Dimitri Moreau (1), Fabrizio Vacca (1), Stefania Vossio (1), Cameron Scott (1),

Alexandria Colaco (2), Jonathan Paz Montoya (3), Charles Ferguson (4), Marc Moniatte (3),

Robert G. Parton (4), Frances M. Platt (2) and Jean Gruenberg* (1).

(1) Department of Biochemistry, University of Geneva, 30 quai E. Ansermet, 1211-Geneva-4, Switzerland.

(2) Department of Pharmacology, University of Oxford, Oxford, OX1 3QT, UK

(3) Mass spectrometry core facility, EPFL, CH-1015 Lausanne, Switzerland

(4) Institute for Molecular Bioscience and Center for Microscopy and Microanalysis, University of Queensland, Brisbane 4072, Australia.

 * To whom correspondence should be addressed: jean.gruenberg@unige.ch.

ABSTRACT

Most cells acquire cholesterol by endocytosis of circulating LDLs. After cholesteryl ester de-esterification in endosomes, free cholesterol is redistributed to intracellular membranes via unclear mechanisms. Our previous work suggested that the unconventional phospholipid lysobisphosphatidic acid (LBPA) may play a role in modulating the cholesterol flux through endosomes. In this study, we used the Prestwick library of FDA-approved compounds in a high content, image-based screen of the endosomal lipids, lysobisphosphatidic acid and LDL-derived cholesterol. We report that thioperamide maleate, an inverse agonist of the histamine H3 receptor HRH3, increases highly selectively the levels of lysobisphosphatidic acid, without affecting any endosomal protein or function that we tested. Our data also show that thioperamide significantly reduces the endosome cholesterol overload in fibroblasts from patients with the cholesterol storage disorder Niemann-Pick type C (NPC), as well as in liver of $Npc1^{-/-}$ mice. We conclude that LBPA controls endosomal cholesterol mobilization and export to cellular destinations, perhaps by fluidifying or buffering cholesterol in endosomal membranes, and that thioperamide has repurposing potential for the treatment of NPC.

INTRODUCTION

Most mammalian cells acquire cholesterol via the uptake of circulating LDLs. After binding to the LDL receptor or other family members, LDLs are delivered to early endosomes where they are uncoupled from their receptor [1]. While the receptor is recycled to the plasma membrane for another round of utilization, LDLs are packaged into maturing multivesicular endosomes, and transported towards late endosomes and lysosomes [2]. In these late endocytic compartments, the LDL particle is disaggregated upon degradation of associated apoproteins, and cholesteryl esters are de-esterified by acidic lipase LIPA. From there, free cholesterol redistributes to intracellular membranes, including the endoplasmic reticulum where it controls the expression of cholesterol-dependent gene via the SREBP pathway [3, 4]. However, the mechanisms that regulate the endosomal cholesterol content, and control its translocation across the endosomal membrane and further export towards other destinations are not clear. When mutated, two genes NPC1 and NPC2 are responsible for the cholesterol storage disease Niemann-Pick type C, but the functions of the NPC1 and NPC2 proteins remain incompletely understood [5].

We previously observed that in NPC cells cholesterol accumulates in late endosomes containing lysobisphosphatidic acid (LBPA) [6, 7], also referred to as bis(monoacylglycero)phosphate (BMP). This atypical phospholipid accounts for approximately 15 Mol% of total phospholipids in the multivesicular late endosomes of BHK cells, where it abounds within intralumenal membranes, and is not detected in other subcellular compartments [7, 8]. In addition to this uncommon distribution, LBPA also exhibits an unusual stereo-configuration [9, 10], and its metabolism is poorly understood [11, 12]. After de-esterification, free LDL-derived cholesterol is incorporated into membrane of LBPA-containing late endocytic compartments. In fact, our data indicate that LBPA plays a direct role in regulating the cholesterol flux through endosomes. Interfering with LBPA functions causes cholesterol accumulation in late endosomes, phenocopying NPC [6, 13], and inhibits Wnt-induced biogenesis of lipid droplets [14]. In this paper, we describe a strategy to identify compounds that influence levels and/or distribution of LBPA. We identify thioperamide as a novel modulator of LBPA levels in late endosomes and show that it decreases the cholesterol overload in fibroblasts from NPC patients and in NPC null mice.

RESULTS

High content screen

We carried out a high content image-based screen to identify compounds that influence LBPA, using a monoclonal antibody against LBPA [7]. Since free LDL-derived cholesterol is released in late endosomes containing LBPA (Fig 1A), and given our observations that cholesterol is functionally linked to LBPA [6], we also monitored cholesterol, using the polyene macrolide filipin, which binds cholesterol and conveniently emits in the UV range. As additional markers for cell segmentation during automated image analysis, we used propidium iodide to label nuclei and cell tracker to label the cytoplasm.

The screen was carried out with the Prestwick library of FDA-approved drugs (http://www.prestwickchemical.com/libraries-screening-lib-pcl.html; and see Table EV1 and Table EV2), because of high chemical and pharmacological diversity, low toxicity, known bioavailability and structures, and also because some target data are available. Fig 1C shows an example of a 384-well plate stained for cholesterol (green) and LBPA (red) with 4 micrographs stitched together per well. As a positive control, the wells in one column were treated with the pharmacological agent U18666A (Fig 1C, right of the plate), a charged sterol analog that mimics NPC [15], binds the NPC1 protein [16], and causes the accumulation of both cholesterol and LBPA in late endosomes [6, 14] (Fig 1E). The broad dynamic range of the detection system and its robustness, as already revealed in our previous RNAi screens with the same detection system [14], are illustrated by the staining with both markers in U18666A-treated vs. control cells (Fig 1C, DMSO left of the plate; Fig 1E)

While most compounds had no effect on the two lipids as anticipated, the majority of the compounds that did have an effect caused a concomitant increase in both cholesterol and LBPA, much like U18666A (Fig 1B). However, several compounds caused an apparent increase in LBPA staining with minimal effect on cholesterol levels — a phenotype particularly striking in cells treated with thioperamide maleate (Fig 1C lower well in the boxed area, and Fig B, pink).

Thioperamide

The selective increase in LBPA, but not cholesterol, is well illustrated in high magnification views of the cells treated with thioperamide (Fig 1E). Automated, unbiased quantification of the screen data confirmed that LBPA staining intensity was increased highly significantly in thioperamide-treated cells without any visible toxic effect, while both LBPA and cholesterol levels increased in the presence of U18666A (Fig 1E) as expected. Similarly, trimeprazine caused a marked increase in LBPA (Fig 1 D-E; light blue in Fig 1B), but also raised cholesterol levels to the same extent as U18666A (Fig 1D-E).

In addition, thioperamide affected equally different cells types of human or rodent origin (Fig 2A). Consistent with our imaging data (Fig 1), a biochemical analysis confirmed that, in marked contrast to U18666A, thioperamide did not affect the levels of free cholesterol, esterified cholesterol and total cholesterol, when compared to controls (Fig 2B). Moreover, automated unbiased quantification further demonstrated that the cholesterol content of individual LBPA-endosomes after thioperamide treatment was very similar to the DMSO controls, and to most samples after treatment with Prestwick compounds (Fig 2C). Finally, an analysis by electron microscopy showed that the ultrastructure of individual endosomes looked very similar in thioperamide-treated cells when compared to controls (Fig EV1A). However, immunogold labeling of cryosections using the anti-LBPA antibody confirmed that the amounts of LBPA in multivesicular late endosomes increased in thioperamide-treated cells (Fig 3A, pseudocoloured individual endosomes and uncolored originals in Fig EV1B; double-blind quantification in Fig 3B).

While differences in staining intensity alone already revealed major differences in the effects of some compounds, the automated image analysis pipeline captured additional parameters, (e.g size, area, integrated intensity, average intensity, object count), to describe and compare the various staining patterns. Given the large set of parameters, the combination of variables was transformed into principal components to best explore the phenotypic space. The principal components analysis (PCA) confirmed that most compounds had no significant effect on cholesterol and LBPA, while all U18666A-treated cells (green, Movie EV1) clustered together far away from the bulk (white, Movie EV1). Interestingly, the PCA also demonstrates that the thioperamide phenotype (pink, Movie

EV1) is set far away from all other compounds, including the positive control U18666A or any compound affecting LBPA or cholesterol. These observations further confirm the notion that the cellular effects of thioperamide are unique and remarkable.

LBPA, cholesterol and endosome distribution

The differences observed in the PCA space between thioperamide vs. U18666A or trimeprazine were not only due to differences in the cholesterol content of LBPA-containing endosomes, but also in their subcellular distribution. After U18666A or trimeprazine treatment, LBPA-positive late endosomes loaded with cholesterol were typically clustered in the perinuclear region (Fig 1E). This distribution agrees well with previous observations by us [13] and others [17, 18] that cholesterol accumulation in NPC cells paralyses late endosomes at the microtubule minus-ends, close to the nucleus. In marked contrast, thioperamide did not seem to cause perinuclear clustering of LBPA-endosomes (Fig 1E), in line with our observations that it did not affect cholesterol (Fig 1C, Fig 2C). Automated unbiased quantification of all cells treated with Prestwick compounds confirmed that U18666A and trimeprazine caused a highly significant increase in perinuclear LBPA staining (Fig 3C). By contrast, thioperamide had essentially no effect on endosome distribution, much like DMSO in controls or most Prestwick compounds (Fig 3C). In addition, counting the number of individual LBPA-positive structures after treatment with Prestwick compounds, showed that thioperamide was present on the side of the distribution opposite to trimeprazine or U18666A (z-factors shown in Fig 3D) — the distribution is relatively noisy because of cell-to-cell variation. Indeed, LBPA-endosomes clustered in the vicinity of the nucleus after trimeprazine or U18666A treatment were no longer well resolved, resulting in an apparent decrease in the number of labeled endosomes.

Endosome functions

We then investigated whether thioperamide had any effect on other endosomal functions. No change was observed in the distribution or amounts of markers of early (EEA1, transferrin receptor) or late (LAMP1, CD63) endocytic compartments (Fig 4A). Similarly, thioperamide did not affect lipid droplets (Fig 4A), the biogenesis of which is regulated by cholesterol flux through endosomes [14]. Neither did it affect the endo-lysosome acidification capacity or on the number of acidic endo-lysosomes (Fig 4C) — the effects of

6

the V-ATPase inhibitor bafilomycin A1 is shown after a short (2h) treatment for comparison. During infection with vesicular stomatitis virus (VSV), the release of viral RNA into the cytoplasm depends on functionally intact endosomes [19] [20], and is inhibited by cholesterol accumulation in endosomes [21]. After incubating cells for 3h with recombinant VSV expressing GFP-tagged P-protein [22] [23] at a low physiologically relevant MOI (1.0), no difference could be observed between thioperamide- and mock-treated control cells (Fig 4B). Moreover, the degradation of the epidermal growth factor (EGF) receptor in cells challenged with EGF, occurred with identical kinetics in cells treated with thioperamide and in controls (Fig 4D; quantification by automated microscopy shown in the bar graph). Altogether, these data demonstrate that thioperamide increases LBPA levels in late endosomes highly selectively without affecting their cholesterol content, and that endosomes and lysosomes of thioperamide-treated cells are functionally intact.

The histamine receptor HRH3

Thioperamide is reported to act as an inverse agonist of the histamine receptor H3 (HRH3) [24]. We thus tested a small library of compounds that target HRH3 or the other members of the same receptor family, HRH1, HRH2 or HRH4. HRH3 is more closely related to HRH4 (37% sequence identity) than to HRH1 or HRH2 (21% sequence identity). Strikingly, 10 out of 12 compounds targeting HRH3 or HRH4, which all act as antagonists or inverse agonists, exhibited a thioperamide-like increase in LBPA without changing cholesterol levels (Fig 5A). For example, pitolisant increased LBPA levels, without affecting cholesterol levels (Fig 2B and Fig 5B), much like thioperamide. These observations strongly argue against the notion that the increase in LBPA levels was caused by some off-target effects of thioperamide, since the chemical scaffolds of these compounds are different. In marked contrast, LBPA accumulation was observed with only 2 out of the 26 compounds against HRH1, and with none of the 5 compounds that target HRH2 (Fig 5A). Neither did histamine (not shown) or any histamine receptor agonist that was tested (Fig 5A).

Further support for the notion that thioperamide targets HRH3 as an inverse agonist came from the observations that levels of LBPA and HRH3 were inversely-correlated. Indeed, in a mixed population of cells expressing GFP-tagged HRH3 (Fig 5F), the cellular intensity of the LBPA signal is skewed towards cells expressing low levels of HRH3-GFP and vice-versa (Fig

7

5G), indicating that LBPA levels are low in cells expressing high HRH3-GFP levels and high in cells expressing low HRH3-GFP levels. These observations were confirmed using cells stably expressing HRH3-GFP. In these cells, HRH3-GFP could be efficiently depleted after knockdown with 4 different siRNAs (Fig 5C, quantification in Fig 5E). Again, LBPA and HRH3-GFP levels were anti-correlated, and HRH3-GFP depletion was accompanied with a concomitant increase in LBPA levels (Fig 5D-E).

Thioperamide reduces cholesterol overload in NPC cells

Cholesterol accumulates in late endocytic compartments of NPC cells, eventually leading to a pathological enlargement of these compartments — a characteristic of lysosomal storage disorders. Concomitant with this increase in endosomal volume, protein and lipid [21], total LBPA levels are also increased [6]. The accumulation of storage materials in NPC endosomes eventually leads to a traffic jam and a collapse of endosomal membrane dynamics [25, 26]. Given the role of LBPA in endosomal cholesterol transport [6, 14, 27], we reasoned that the capacity of LBPA to accommodate — or buffer — excess cholesterol may eventually become limiting in NPC endosomes.

To test the effects of thioperamide in NPC cells, we used three fibroblast lines obtained from patients with well-established mutations in the NPC1 or NPC2 gene. In all three cell lines, thioperamide caused after 72h a very significant decrease in cholesterol levels (Fig 6A, quantification in Fig 6B at 72h). In contrast to control cell lines (Fig 1 and Fig 2A), LBPA levels were also decreased in NPC cell lines after a 72h treatment (Fig 6B). We hypothesized that the effects of the drug on LBPA levels may be obscured in NPC cells by the beneficial decrease in storage of cholesterol and other lipids including LBPA. Indeed, a significant increase in LBPA levels was transiently observed at a shorter time-point, before changes in cholesterol could be detected (Fig 6B at 48h). The simplest interpretation may be that, much like in other cell types, thioperamide increases LBPA levels in NPC cells, thus facilitating cholesterol mobilization, consistent with previous findings [27], which in turn reduces storage materials in endosomes and restores physiological levels of LBPA and other lipids.

Biochemical quantification showed that cholesterol levels normalized to total cellular lipids were efficiently reduced by thioperamide treatment of all 3 NPC cell lines (Fig 6C). We compared the reduction in cholesterol levels to treatment with cyclodextrin, currently considered to be one of the — if not the — most efficient protocol to reduce cholesterol levels in cultured cells [5, 28] . Cyclodextrin also decreases the progression of neurological disorders in NPC1 patients after intrathecal injection [29]. Remarkably, biochemical quantification revealed that thioperamide reduced cholesterol levels in all three NPC cell lines as efficiently as cyclodextrin (Fig 6C).

Effects of thioperamide in *Npc1*$^{-/-}$ mice

Finally, we tested the effects of thioperamide in mice lacking NPC1, which model the most aggressive early onset form of the disease [30]. As anticipated, the liver of *Npc1*$^{-/-}$ mice showed significant accumulation of cholesterol, approximately 20X higher than livers from WT littermates (Fig 6D). LBPA was quantified by mass spectrometry after efficient separation from phosphatidylglycerol (PG), because the two lipids are isobaric (Fig EV2A). Much like cholesterol, LBPA also accumulated approximately 10X (Fig 6E). Interestingly, the mass spectrometry analysis also revealed the presence of a triple acylated version of LBPA, semilysobisphosphatidic acid (sLBPA) [31], which could be well separated from LBPA and PG (Fig EV2B). sLBPA also accumulated significantly, increasing from less than 0.05% of total phospholipids in WT liver to 0.8 % in *Npc1*$^{-/-}$ liver (Fig EV3A) — a value close to the physiological levels of LBPA in WT liver (1.0 % of total phospholipids). Moreover, our lipidomic analysis revealed a dramatic remodeling of the acyl chain composition of both LBPA (Fig EV4A) and sLBPA (Fig EV4B) in *Npc1*$^{-/-}$ mouse liver, characterized by shorter acyl chains and a reduced number of double bonds, confirming the notion that a metabolic relationship exists between LBPA and sLBPA [31]. In marked contrast to LBPA and sLBPA, the total relative amounts of other phospholipids were not significantly affected in *Npc1*$^{-/-}$ mouse liver (Fig EV3C). Neither was the acyl chain composition of other phospholipids, as illustrated with phosphatidylcholine (Fig. S5A) and phosphatidlyethanolamine (Fig EV5B). These observations further strengthen the notion that LBPA and cholesterol are closely linked functionally.

WT and $Npc1^{-/-}$ mice were then treated with thioperamide. The treatment started at weaning (3 weeks of age) and the mice were sacrificed at 9 weeks, to minimize suffering. LBPA was marginally decreased in drug-treated $Npc1^{-/-}$ liver (Fig 6E), and sLBPA unaffected (Fig EV3A), while the acyl chain composition remained unchanged (Fig EV4A-B). Strikingly, however, the cholesterol levels in the $Npc1^{-/-}$ mouse liver were significantly reduced by the thioperamide treatment (Fig 6D and F), as in NPC fibroblasts (Fig 6A-C). Altogether, these data suggest that in NPC cell lines and $Npc1^{-/-}$ liver cells thioperamide facilitates cholesterol mobilization, presumably by transiently increasing LBPA levels, similar to other cells (Fig 1-3), which in turn reduces storage materials in endosomes, including LBPA and other lipids. The distribution of LBPA vs cholesterol in $Npc1^{-/-}$ mice may well reflect the end-point balance between thioperamide-induced increase in LBPA and the beneficial effects of the treatment on the compartment overload. In any case, our data demonstrate that thioperamide reduces the cholesterol storage phenotype both in NPC fibroblasts and $Npc1^{-/-}$ mice.

DISCUSSION

In conclusion, we find that LBPA levels i) are increased by thioperamide and other inhibitors or inverse agonists of the HRH3 receptor that do not share a common backbone, and ii) are inversely correlated with the levels of GFP-HRH3 expression. We also find that thioperamide does not affect any endosomal protein or function that was tested, including acidification, lysosomal degradation and enveloped virus infection. Finally, we find that thioperamide decreases cholesterol overload in both NPC1 and NPC2 mutant cells as well as in $Npc1^{-/-}$ mouse liver.

More work will be needed to establish unambiguously what is the mode of action of thioperamide, as well as the link between LBPA and cholesterol. However, some speculations are already possible. First, the notion that thioperamide acts by modulating the activity of the NPC1 or NPC2 proteins can be ruled out, given the effects of the drug in NPC cells and mice. It also seems fairly unlikely that thioperamide exerts its direct and selective effect on cholesterol, by modulating the biochemical or biophysical properties of the cholesterol-laden bilayer after partitioning into endosomal (LBPA-containing) membranes. Indeed, the drug raises LBPA levels specifically without affecting any other endosomal function or protein. Moreover, this view is not easily reconciled with observations that LBPA levels are also increased by other inhibitors of the HRH3 receptor that do not share a common backbone with thioperamide. Hence, the simplest interpretation is that binding of thioperamide to the HRH3 receptor on the cell surface as inverse agonists [24], increases LBPA levels by stimulating biosynthesis or inhibiting turnover — an issue not easily solved since the metabolic regulation of LBPA remains mysterious and the enzymes involved in biosynthesis and turnover are not known [11, 12]. High LBPA levels in turn may contribute to fluidify or buffer cholesterol in endosomal membranes, thereby facilitating its mobilization and subsequent export to cellular destinations.

In NPC cells, before the addition of thioperamide, the levels of LBPA are already strongly elevated [6] (see Fig 6D), as part of the general expansion of late endosome volume, protein and lipid [21] . This enlargement of the endosomal system presumably reflects the attempt to compensate for the accumulation of storage materials. Eventually, however, the system

collapses under the excess load, leading to a traffic jam and a breakdown of endosomal membrane dynamics [25, 26]. Given its role in endosomal cholesterol transport [6, 14, 27], we propose that LBPA then becomes limiting, because its capacity to accommodate — or buffer — excess cholesterol in NPC endosomes is overwhelmed. Alternatively, LBPA may play a more direct role in cholesterol mobilization and transport. In any case, it is also tempting to speculate that the highly selective changes in LBPA and sLBPA acyl chain composition — shorter chains and reduced number of double bonds — observed in NPC mouse liver reflect some additional adjustment in membrane chemical and physical properties to better accommodate changes due to cholesterol accumulation [32-35].

At first sight, it may appear counter-intuitive that thioperamide acts in NPC cells and mice via LBPA, since the drug decreases LBPA levels in NPC cells after 72h (Fig 6B) and in $Npc1^{-/-}$ mouse liver at least to some extent (Fig 6E). However, our model predicts that LBPA will only be transiently increased in NPC cells. High LBPA levels will alleviate cholesterol overload, which in turn will reduce storage and revert the cell response to the endosome overload, resulting in decreased levels of LBPA and other endosomal lipids and proteins. Indeed, as predicted, a significant increase in LBPA levels was transiently observed in NPC cells at a shorter time-point, before changes in cholesterol could be detected (Fig 6B at 48h). In NPC mice, the effects of the drug are also likely to be masked by the beneficial decrease in storage of cholesterol and other lipids including LBPA. Consistent with previous findings [27], we conclude that in NPC cells much like in other cell types, thioperamide increases LBPA levels, which helps buffer membrane cholesterol and reduce storage materials in endosomes. Since a very limited number of strategies only are emerging as possible treatment for NPC [29, 36-38], we believe that our study of the FDA-approved compound thioperamide provide exciting novel perspectives for the treatment of NPC.

METHODS

Reagents and cells

We used the following mouse monoclonal antibodies against: transferin receptor (13-6800, Invitrogen, 1/200); CD63 [39]; LBPA (1/100) [7]; EGF receptor (555996, BD Biosciences, 1/200). We also used rabbit monoclonal antibodies against Lamp1 (D2D11, 9091, Cell signaling, 1/500); and rabbit polyclonal antibody against EEA1 (ALX-210-239, ENZO life science, 1/400); as well as affinity-purified donkey antibodies against mouse IgG, alexa488-labeled (715,545,151, Jackson Immunoresearch, 1/200) and against rabbit IgG, Cy3-labeled (ref: 711,165,152, Jackson Immunoresearch, 1/200). We obtained filipin (F4767) from Sigma; BODIPY-493/503 Methyl Bromide (used at 1/1000 from 1 mg/ml ethanol stock) and CellTracker green (C2925) from Thermo Fisher Scientific; RNAse (12091-021) and propidium iodide from (Ref. P3566) from Invitrogen.

The three NPC fibroblast patient cell lines were obtained from Coriell Institute, NIGMS Human Genetic Cell Repository (reference numbers are indicated in the text and figures). All details about the NPC gene mutations can be found on the Coriell Institute website (https://www.coriell.org/1/NIGMS). When indicated, the cells were treated with 10μM thioperamide or DMSO (1/2000) for 72h and imaged by automated microscope.

HCS Screen

The compound screen was carried out in Hela MZ cells (provided by Marino Zerial, MPI-CBG, Dresden) and A431 cells, cultured as described [14]. In the screen, we used BD Falcon 384 well imaging plates (ref. 353962). In each well, cells in a 20μl suspension (3500 cell/well) were seeded on top of 5μl solution containing 10μM compound. In each plate, DMSO control was added in all wells of column 2 and U18666A in all wells of column 23. Plates were incubated for 18h before fixation (4% PFA) and staining using an automated plate washer (Biotek EL406). Cells were then incubated for 30min with Celltracker green and stained as follows. Step 1: 6C4 monoclonal antibody against LBPA, 1/100, saponin 0.05%, RNAse 1/100, BSA 1%, in PBS, incubation for 1h. Step 2: propidium iodide, filipin 1/50, Cy5-labeled secondary antibody against mouse IgG, 1/200, incubation for 30min. Image

acquisition was performed immediately after staining on a BD pathway 455 automated microscope with the 20X objective. Four images were captured per well.

Image analysis with MetaXpress Custom Module Editor

To analyze and quantify the LBPA and free cholesterol cell content, we used the MetaXpress Custom Module editor software to first segment the image and generate relevant masks, which were then applied on the fluorescent images to extract relevant measurements. In the first step, the cell was segmented by using the nuclei (propidium iodide) channel and the cytoplasm (CellTracker green) channel. To facilitate segmentation of LBPA endosome, we applied the top hat deconvolution method to the LBPA channel (Cy5) to reduce the background noise and highlight bright granules. LBPA endosomes were segmented from the deconvoluted image. When indicated, we used a perinuclear mask to specifically quantify the LBPA and cholesterol (flipin) signals in the perinuclear area. The final masks are then applied to the original fluorescent images and 50 measurements per cell (e.g. size, area, integrated intensity, average intensity, object count) are extracted. The same analysis pipeline has been applied to all images.

Data analysis with AcuityXpress

All plates were annotated with the compound library using AcuityXpress. Data set were normalized (Z-score) and analyzed using the same software to generate all screen graphs and PCA. Compounds displaying more than 40% toxicity were excluded from the data analysis.

EGF receptor degradation

HeLa-MZ were starved in serum free medium for 4h and treated with 100nM EGF as indicated [40]. Cells were then fixed and stained with antibodies to the EGF receptor, followed by fluorescently labeled secondary antibodies. The EGF receptor signal was then quantified by automated microscopy using the ImageXpress® confocal microscope (Molecular Devices™) after segmentation of the granular structures containing the EGFR signal [41], using Custom Module Editor™ from MetaXpress™. The obtained mask was then applied to the EGF receptor fluorescent micrographs and the integrated intensity (sum of all pixel intensities) is extracted for each cell (approx. 5000 cells analyzed per condition).

HRH3 stable cell

The HeLa MZ HRH3-GFP stable cell line has been generated using the gateway pLenti 6.3 V5CT vector backbone. Lentivirus have been prepared as follow: $6x10^3$ HEK293T cells were seeded into 10 cm dishes pre-coated for 15min with 0.001% poly-L-lysine (1:10 dilution of 0.01% stock). Cells were incubated for 6h at 37˚C, 5% CO_2 in medium containing 10% FBS before transfection. The transfection mix contained 15µl Lipofectamine 2000, plasmids (pLenti6.3-V5CT-HRH3-GFP 15µg, pLP1 10µg, pLP2 10µg, pLP-VSV-G 10µg) in OptiMEM (500µl final). The reactions were mixed and incubated for 20min at room temperature. After 48h, the medium was aspirated and exchanged with fresh medium. Then 24h later, the medium was collected, filtered (0.45µm) and directly added onto target cells (at 40% confluency). The target cells were then cultured for 48h before detecting expression. At that point, the medium was changed and cells treated with blasticidin (20ug/ml) for the first selection. Clone selection was carried out in the presence of 5µg/ml blasticidin by dilution in 384 well-plates and clones were analyzed by automated microscope.

Lipid extraction for Mass Spec

Cells (near confluency in 6-cm plastic dishes) were scraped off the dish in PBS and sedimented for analysis. Alternatively, lyophilized homogenized liver tissue (7,5 mg) were resuspended in 100µl cold water before addition of 360µl methanol and the internal standard ergosterol (20 nmol). Next, 1.2ml 2-methoxy-2-methylpropane (MTBE) was added and lipids were extracted by vortexing at 4°C for 10min followed by 1h shaking at room temperature to allow complete lipid partitioning [42]. A total of 200µl water was added to induce phase separation, and the upper phase was collected and dried. Total phosphates were quantified with an ammonium Molybdate colorimetric assay [43].

Mass spectrometry

Membrane cholesterol and cholesteryl ester amounts were normalized and calibrated using the total phosphate content and the integrated signal of a spiked ergosterol standard, as previously described [14]. For phospholipid analysis, dried lipid samples were re-dissolved in chloroform–methanol (1:1 v/v). Separation was performed on a HILIC Kinetex column (2.6µm, 2.1 × 50mm2) on a Shimadzu Prominence UFPLC xr system (Tokyo, Japan): mobile

phase A was acetonitrile:methanol 10:1 (v/v) containing 10mM ammonium formate and 0.5% formic acid; mobile phase B was deionized water containing 10mM ammonium formate and 0.5% formic acid. The elution of the gradient began with 5%B at a 200µL/min flow and increased linearly to 50% B over 7 min, then the elution continued at 50% B for 1.5 min and finally the column was re-equilibrated for 2.5 min. The sample was injected in 2µL chloroform:methanol 1:2 (v/v). Data were acquired in full scan mode at high resolution on a hybrid Orbitrap Elite (Thermo Fisher Scientific, Bremen, Germany). The system was operated at 240'000 resolution (m/z 400) with an AGC set at 1.0E6 and one microscan set at 10ms maximum injection time. The heated electro spray source HESI II was operated in positive mode at a temperature of 90°C and a source voltage at 4.0KV. Sheath gas and auxiliary gas were set at 20 and 5 arbitrary units respectively while the transfer capillary temperature was set to 275°C. The mass spectrometry data were acquired with LTQ Tuneplus2.7SP2 and treated with Xcalibur 4.0QF2 (Thermo Fisher Scientific). Lipid identification was carried out with Lipid Data Analyzer II (LDA v. 2.5.2, IGB-TUG Graz University) [44]. Peaks were identified by their respective retention time, m/z and intensity. Instruments were calibrated to ensure a mass accuracy lower than 3ppm. Data visualization was improved with the LCMSexplorer web tool hosted at EPFL (https://gecftools.epfl.ch/lcmsexplorer). We could clearly show the separation of LBPA from the isobaric lipid PG, as already described by others with HILIC column [45], which allows unambiguous quantification of the two lipids (fig. S2).

Enzymatic Cholesterol Quantification

Cholesterol content in liver samples was quantified enzymatically using the Amplex Red cholesterol kit assay (Molecular probes; A12216). Liver lipids extracted with MTBE were dried, resuspended in pure methanol and then directly diluted in the assay buffer. The assay in a 96-well plate format was according to the manufacturer's instructions.

Mouse lipid analysis

BALBc/NPC[nih] mice were bred as heterozygotes to generate $Npc1^{-/-}$ mice and control genotypes. Mice were bred and housed under non-sterile conditions, with food and water available ad lib. All experiments were conducted using protocols approved by the UK Home Office Animal Scientific Procedures Act, 1986. $Npc1^{-/-}$ and $Npc1^{+/+}$ mice (n = 6 males and 6

females) were treated with the compound in the drinking water (at 8.8 mg/L, corresponding to 2mg/kg/day). Treatment started at weaning (3 weeks of age) and mice were sacrificed at 9 weeks of age by intraperitoneal injection with an overdose of phenobarbital Care was taken to minimize suffering through euthanizing the animals once liver enlargement was unambiguously detected by visual inspection (i.e. 3 weeks after initiation of treatment).

Other methods

Transfection with siRNAs was performed according to manufacturers' instructions using RNAiMAX (ThermoFisher Scientific). We performed reverse transfection by seeding 80μl HeLa cells (2 x 103 cells/well) onto a 20 ul mix of siRNA (10nM) and transfection reagent. Hela MZ were infected with VSV [19] using a Biotek™ EL406 plate washer, fixed with 4% PFA and stained with DAPI, and images were acquired with the IXM™ microscope and analysed with MetaXpress™ to quantify infected cells. The cholesterol content of liver extracts was measured enzymatically using the Amplex Red kit (Molecular probes). Dried lipid samples were re-dissolved in pure methanol, sonicated for 5min and diluted in the assay buffer for quantification. Electron microscopy after plastic embedding for HRP analysis [46] or after immunogold labeling of cryosections [47] has been described. Quantitation of LBPA labeling of sections from control (DMSO-treated) or thioperamide-treated cells was performed in a double-blind fashion by counting the number of late endosomes/lysosomes (defined by multivesicular morphology; see images) containing ≤5 or ≥6 gold particles.

ACKNOWLEDGEMENTS

AUTHOR CONTRIBUTIONS

DM designed the experiments, carried out the screen and the characterization as well as the data analysis, and wrote the manuscript.

FV contributed to the lipid analysis

SV contributed to the screen

CS contributed to data analysis

AC carried out the experiments with mice

JPM contributed to the mass spectrometry analysis

CF contributed to the electron microscopy analysis

MM contributed to the mass spectrometry analysis

RGP contributed to the electron microscopy analysis

FP contributed to the experiments with mice

JG designed the experiments and wrote the manuscript

COMPETING INTERESTS

The authors declare no competing interests.

REFERENCES

1.   Goldstein JL, Brown MS (2009) The LDL receptor. *Arterioscler Thromb Vasc Biol* **29**: 431-8

2.   Scott CC, Vacca F, Gruenberg J (2014) Endosome Maturation, Transport and Functions. *Semin Cell Dev Biol* **31**: 2-10

3.   Brown MS, Goldstein JL (1997) The SREBP pathway: regulation of cholesterol metabolism by proteolysis of a membrane-bound transcription factor. *Cell* **89**: 331-40

4.   Brown MS, Radhakrishnan A, Goldstein JL (2017) Retrospective on Cholesterol Homeostasis: The Central Role of Scap. *Annu Rev Biochem*

5.   Rosenbaum AI, Maxfield FR (2011) Niemann-Pick type C disease: molecular mechanisms and potential therapeutic approaches. *J Neurochem* **116**: 789-95

6.   Kobayashi T, Beuchat MH, Lindsay M, Frias S, Palmiter RD, Sakuraba H, Parton RG, Gruenberg J (1999) Late endosomal membranes rich in lysobisphosphatidic acid regulate cholesterol transport. *Nature cell biology* **1**: 113-8

7.   Kobayashi T, Stang E, Fang KS, de Moerloose P, Parton RG, Gruenberg J (1998) A lipid associated with the antiphospholipid syndrome regulates endosome structure and function. *Nature* **392**: 193-7

8.   Kobayashi T, Beuchat MH, Chevallier J, Makino A, Mayran N, Escola JM, Lebrand C, Cosson P, Gruenberg J (2002) Separation and characterization of late endosomal membrane domains. *J Biol Chem* **277**: 32157-64

9.   Brotherus J, Renkonen O, Herrmann J, Fisher W (1974) Novel stereochemical configuration in lysobisphosphatidic acid of cultured BHK cells. *Chem Phys Lipids* **13**: 178-182

10.   Tan HH, Makino A, Sudesh K, Greimel P, Kobayashi T (2012) Spectroscopic evidence for the unusual stereochemical configuration of an endosome-specific lipid. *Angewandte Chemie* **51**: 533-5

11.   Amidon B, Schmitt JD, Thuren T, King L, Waite M (1995) Biosynthetic conversion of phosphatidylglycerol to sn-1:sn-1' bis(monoacylglycerol) phosphate in a macrophage-like cell line. *Biochemistry* **34**: 5554-60

12. Hullin-Matsuda F, Kawasaki K, Delton-Vandenbroucke I, Xu Y, Nishijima M, Lagarde M, Schlame M, Kobayashi T (2007) De novo biosynthesis of the late endosome lipid, bis(monoacylglycero)phosphate. *J Lipid Res* **48**: 1997-2008

13. Lebrand C, Corti M, Goodson H, Cosson P, Cavalli V, Mayran N, Faure J, Gruenberg J (2002) Late endosome motility depends on lipids via the small GTPase Rab7. *Embo J* **21**: 1289-300

14. Scott CC, Vossio S, Vacca F, Snijder B, Larios J, Schaad O, Guex N, Kuznetsov D, Martin O, Chambon M*, et al.* (2015) Wnt directs the endosomal flux of LDL-derived cholesterol and lipid droplet homeostasis. *EMBO Rep* **16**: 741-52

15. Liscum L, Faust JR (1989) The intracellular transport of low density lipoprotein-derived cholesterol is inhibited in Chinese hamster ovary cells cultured with 3- beta-[2-(diethylamino)ethoxy]androst-5-en-17-one. *J Biol Chem* **264**: 11796-806

16. Lu F, Liang Q, Abi-Mosleh L, Das A, De Brabander JK, Goldstein JL, Brown MS (2015) Identification of NPC1 as the target of U18666A, an inhibitor of lysosomal cholesterol export and Ebola infection. *Elife* **4**

17. Ko DC, Gordon MD, Jin JY, Scott MP (2001) Dynamic movements of organelles containing Niemann-Pick C1 protein: NPC1 involvement in late endocytic events. *Mol Biol Cell* **12**: 601-14

18. Zhang M, Dwyer NK, Love DC, Cooney A, Comly M, Neufeld E, Pentchev PG, Blanchette-Mackie EJ, Hanover JA (2001) Cessation of rapid late endosomal tubulovesicular trafficking in Niemann-Pick type C1 disease. *Proc Natl Acad Sci U S A* **98**: 4466-71

19. Le Blanc I, Luyet PP, Pons V, Ferguson C, Emans N, Petiot A, Mayran N, Demaurex N, Faure J, Sadoul R*, et al.* (2005) Endosome-to-cytosol transport of viral nucleocapsids. *Nature cell biology* **7**: 653-64

20. Lozach PY, Huotari J, Helenius A (2011) Late-penetrating viruses. *Current opinion in virology* **1**: 35-43

21. Sobo K, Le Blanc I, Luyet PP, Fivaz M, Ferguson C, Parton RG, Gruenberg J, van der Goot FG (2007) Late endosomal cholesterol accumulation leads to impaired intra-endosomal trafficking. *PLoS One* **2**: e851

22. Das SC, Nayak D, Zhou Y, Pattnaik AK (2006) Visualization of intracellular transport of vesicular stomatitis virus nucleocapsids in living cells. *Journal of virology* **80**: 6368-77

23.   Luyet PP, Falguières T, Pons V, Pattnaik AK, Gruenberg J (2008) The ESCRT-I subunit Tsg101 controls endosome-to-cytosol release of viral RNA. *Traffic* **9**: 2279-90

24.   Tiligada E, Zampeli E, Sander K, Stark H (2009) Histamine H3 and H4 receptors as novel drug targets. *Expert Opin Investig Drugs* **18**: 1519-31

25.   Simons K, Gruenberg J (2000) Jamming the endosomal system: lipid rafts and lysosomal storage diseases. *Trends Cell Biol* **10**: 459-62

26.   Liscum L (2000) Niemann-Pick type C mutations cause lipid traffic jam. *Traffic* **1**: 218-25

27.   Chevallier J, Chamoun Z, Jiang G, Prestwich GD, Sakai N, Matile S, Parton RG, Gruenberg J (2008) Lysobisphosphatidic acid controls endosomal cholesterol levels. *J Biol Chem* **283**: 27871-80

28.   Vance JE, Peake KB (2011) Function of the Niemann-Pick type C proteins and their bypass by cyclodextrin. *Curr Opin Lipidol* **22**: 204-9

29.   Ory DS, Ottinger EA, Farhat NY, King KA, Jiang X, Weissfeld L, Berry-Kravis E, Davidson CD, Bianconi S, Keener LA*, et al.* (2017) Intrathecal 2-hydroxypropyl-beta-cyclodextrin decreases neurological disease progression in Niemann-Pick disease, type C1: a non-randomised, open-label, phase 1-2 trial. *Lancet* **390**: 1758-1768

30.   Pentchev PG, Gal AE, Booth AD, Omodeo-Sale F, Fouks J, Neumeyer BA, Quirk JM, Dawson G, Brady RO (1980) A lysosomal storage disorder in mice characterized by a dual deficiency of sphingomyelinase and glucocerebrosidase. *Biochimica et biophysica acta* **619**: 669-79

31.   Brotherus J, Niinioja T, Sandelin K, Renkonen O (1977) Experimentally caused proliferation of lysosomes in cultured BHK cells involving an increase of biphosphatidic acids and triglycerides. *J Lipid Res* **18**: 379-88

32.   Harroun TA, Katsaras J, Wassall SR (2006) Cholesterol hydroxyl group is found to reside in the center of a polyunsaturated lipid membrane. *Biochemistry* **45**: 1227-33

33.   Barelli H, Antonny B (2016) Lipid unsaturation and organelle dynamics. *Curr Opin Cell Biol* **41**: 25-32

34.   van Meer G (2011) Dynamic transbilayer lipid asymmetry. *Cold Spring Harb Perspect Biol* **3**

35.   Marquardt D, Kucerka N, Wassall SR, Harroun TA, Katsaras J (2016) Cholesterol's location in lipid bilayers. *Chem Phys Lipids* **199**: 17-25

36.   Lyseng-Williamson KA (2014) Miglustat: a review of its use in Niemann-Pick disease type C. *Drugs* **74**: 61-74

37.   Helquist P, Maxfield FR, Wiech NL, Wiest O (2013) Treatment of Niemann--pick type C disease by histone deacetylase inhibitors. *Neurotherapeutics* **10**: 688-97

38.   Kirkegaard T, Gray J, Priestman DA, Wallom KL, Atkins J, Olsen OD, Klein A, Drndarski S, Petersen NH, Ingemann L*, et al.* (2016) Heat shock protein-based therapy as a potential candidate for treating the sphingolipidoses. *Sci Transl Med* **8**: 355ra118

39.   Vischer UM, Wagner DD (1993) CD63 is a component of Weibel-Palade bodies of human endothelial cells. *Blood* **82**: 1184-91

40.   Brankatschk B, Wichert SP, Johnson SD, Schaad O, Rossner MJ, Gruenberg J (2012) Regulation of the EGF Transcriptional Response by Endocytic Sorting. *Science Signal* **5**: ra21

41.   Wallabregue A, Moreau D, Sherin P, Moneva Lorente P, Jarolimova Z, Bakker E, Vauthey E, Gruenberg J, Lacour J (2016) Selective Imaging of Late Endosomes with a pH-Sensitive Diazaoxatriangulene Fluorescent Probe. *J Am Chem Soc* **138**: 1752-5

42.   Matyash V, Liebisch G, Kurzchalia TV, Shevchenko A, Schwudke D (2008) Lipid extraction by methyl-tert-butyl ether for high-throughput lipidomics. *J Lipid Res* **49**: 1137-46

43.   Lanzetta PA, Alvarez LJ, Reinach PS, Candia OA (1979) An improved assay for nanomole amounts of inorganic phosphate. *Anal Biochem* **100**: 95-7

44.   Hartler J, Trotzmuller M, Chitraju C, Spener F, Kofeler HC, Thallinger GG (2011) Lipid Data Analyzer: unattended identification and quantitation of lipids in LC-MS data. *Bioinformatics* **27**: 572-7

45.   Scherer M, Schmitz G, Liebisch G (2010) Simultaneous quantification of cardiolipin, bis(monoacylglycero)phosphate and their precursors by hydrophilic interaction LC-MS/MS including correction of isotopic overlap. *Anal Chem* **82**: 8794-9

46.   Parton RG, Schrotz P, Bucci C, Gruenberg J (1992) Plasticity of early endosomes. *J Cell Sci* **103 (Pt 2)**: 335-48

47.   Griffiths G, McDowall A, Back R, Dubochet J (1984) On the preparation of cryosections for immunocytochemistry. *J Ultrastruct Res* **89**: 65-78

FIGURE LEGENDS

Figure 1.

(A) Outline of endocytic cholesterol transport.

After endocytosis by the LDL receptor, LDL are delivered to early and then late endosomes. Free cholesterol is released in late endosomes and then exported to its cellular destinations.

(B) Screen data plot

The plot shows the integrated intensity of LBPA vs. filipin (cholesterol) staining in all cells of each well analyzed in the screen (average of replicates). The cells treated with U18666A , thioperamide maleate and trimeprazine tartrate are indicated, as well as the DMSO controls.

(C) Example of a 384-well plate treated with compounds.

The panel shows the staining with filipin (free cholesterol in green pseudo-colour) and anti-LBPA antibodies (red). The leftmost column shows control wells treated with DMSO only, and the right penultimate column shows wells treated with U18666A

(D) Integrated intensity of cholesterol and LBPA staining.

The integrated intensity of cholesterol (filipin in green) and LBPA (red) staining in all cells of the indicated samples is quantified after normalization to the DMSO controls.

(E) Effects of U18666A, thioperamide and trimeprazine, compared with controls.

Cells treated with the indicated compounds or with DMSO alone for 18h at 37°C, were processed for immunofluorescence microscopy. Low magnification views are shown after staining with anti-LBPA antibodies (red), filipin (green pseudo-color) and DAPI (blue). The bar is XXX μm.

Figure 2.

(A) Thioperamide treatment of tissue culture cells.

BHK, CHO and HeLa cells were treated with thioperamide and processed as in Fig 1E. Low magnification views are shown after staining with anti-LBPA antibodies (green) and DAPI (blue).

(B) Cholesterol quantification by mass spectrometry

A431 cells were treated with DMSO alone, pitolisant (Pito), thioperamide (thio) or U18666A (U18) for 18h at 37°C. After extraction, free cholesterol, cholesteryl esters and total cholesterol were quantified by mass spectrometry, and normalized to the DMSO controls.

(C) Screen data plot of the cholesterol content of LBPA-endosomes.

Automated unbiased quantification of the filipin integrated fluorescence signal (cholesterol content) in LBPA-containing endosomes, after treatment with each compound of the Prestwick library. The fluorescence signal of LBPA-endosomes was used to segment the imaged and generate a mask, which was then applied on the micrographs to quantify the integrated intensity of filipin staining. The samples treated with thioperamide (pink), trimeprazine (light blue), DMSO (red) and U18666A (green) are indicated.

Figure 3.

(A-B) Immunogold labelling with anti-LBPA antibodies.

HeLa MZ cells were treated or not with thioperamide for 18h and processed for electron microscopy. Cryosections were labelled with anti-LBPA antibodies followed by 5nm protein A-gold (C). Multivesicular endosomes are pseudocoloured (see Fig EV1 for uncoloured images). Bars, 200nm. The data in (A) were quantified and the proportion of late endosomes containing ≤ 5 or >6 gold particles is shown in (B).

(C) Distribution of LBPA-containing endosomes in the perinuclear region.

Automated unbiased quantification of LBPA fluorescence in the perinuclear region of the cells, after treatment with each compound of the Prestwick library as in Fig 2C. The integrated intensity of the LBPA fluorescence signal was measured within a mask of the perinuclear region in each cell, calculated from the nuclei DAPI-staining. The samples treated with thioperamide (pink), trimeprazine (light blue), DMSO (red) and U18666A (green) are indicated.

(D) Number of perinuclear LBPA endosomes.

The number of individual LBPA-positive structures was measured in the perinuclear region as in (A). The z-factors are shown to evaluate the distribution of endosomes containing LBPA; color code as in (A).

Figure 4.

(A) Analysis of endosomal comaprtments by immuo-fluorescence.

HeLa MZ cells were treated or not with thioperamide or 18h and processed for immunofluorescence microscopy after labelling with DAPI (nuclei) and antibodies against the indicated proteins. Lipid droplets were labelled with Bodipy [14]. The bar graph shows the quantification by automated microscopy of the intensity of the fluorescence signals; TfR: transferrin receptor.

(B) Infection with vesicular stomatitis virus (VSV)

HeLa cells treated or not with thioperamide for 15h were further incubated for 3h in the presence of the drug and recombinant VSV expressing a GFP-tagged version of the viral phosphoprotein (P-eGFP) [22] [23] at low physiologically relevant MOI (1.0). Cells were labeled with DAPI (nuclei) and analyzed by fluorescence microscopy. The bar graph shows the percentage of infected cells after quantification by automated microscopy.

(C) Acidic pH of endosomes and lysosomes

HeLa cells were treated or not with thioperamide as in (A) and incubated with LysoTracker to label acidic compartments. For comparison, cells were also treated for a short (2h) period with the V-ATPase inhibitor Bafilomyin A1. Cells were then labelled with DAPI (nuclei) and processed for fluorescence microscopy. The bar graphs show the integrated intensity (left) and number (right) of labelled structures after quantification by automated microscopy.

(D) EGF-receptor degradation

HeLa MZ cells treated or not with thioperamide as in (A) were challenged with 100nM EGF for 60min and further incubated at 37°C for the indicated time periods with or without the drug, up to a total time period of 18h. Cells were labelled with DAPI (nuclei) and antibodies against the EGF receptor and processed for fluorescence microscopy. The panels show examples of the EGF receptor distribution after 60min. The bar graph shows the integrated intensity of the labelled structures after quantification by automated microscopy.

Figure 5.

(A) Effects of compounds that target histamine receptor family members.

Cells were treated with a small library of compounds that target members of the histamine receptor family, as antagonists (HRH1, HRH2, HRH3 and HRH4) or agonists, and analysed by automated microscopy after labeling with DAPI and antibodies against LBPA**.** Compounds that increased LBPA staining intensity, like thioperamide (Fig 1) or pitolisant (Fig 5B) are green, while compounds without effects are red.

(B) Effect of Pitolisant on LBPA.

HeLa MZ cells treated or not with pitolisant for 18h at 37°C were labeled with DAPI and anti-LBPA antibodies and analysed by fluorescence microscopy.

(C-E) LBPA intensity in cells expressing or not HRH3-GFP

HeLa MZ cells stably expressing HRH3-GFP grown in 384-well plates were separately treated, with 4 different siRNAs that target HRH3 (siHRH3#1; siHRH3#2; siHRH3#3; siHRH3#4) or with control non-target (siNT) siRNA (C). HRH3-GFP was analysed by fluorescence microscopy in 4 rows of cells per condition; micrographs are stitched together in the montage. Panel D shows an example of cells treated with siHRH3#2 or siNT, and then labelled with DAPI and antibodies against LBPA. Cells treated as in (C) and labelled with DAPI and antibodies against LBPA as in (D), were analysed by automated microscopy and the integrated intensities of LBPA (left panel) and HRH3-GFP (right panel) signals are compared (E).

(F-G) LBPA intensity in cells varying amounts of HRH3-GFP

After transfection with HRH3-GFP, uncloned stably expressing cells (F) were labelled with anti-LBPA antibodies and analysed by automated microscopy (F). Unbiased quantification (G) shows the inverse correlation between HRH3-GFP expression (high expressing cells in green) and the integrated intensity of LBPA staining (high LBPA labelling in red).

Figure 6.

(A) Treatment of NPC fibroblasts and NPC null mice with thioperamide.

Fibroblast lines obtained from patients with well-established heterozygote mutations in the NPC1 (GM17912 line: NPC1 P1007A / T1036M; GM17911 line: NPC1 I1061T / T1036M) or with a homozygote mutation in the NPC2 gene (GM17910 line: C93F / C93F) were treated or not for 72h with thioperamide, stained with filipin (cholesterol) and analysed by fluorescence microscopy.

(B) Quantification of cholesterol and LBPA staining in NPC fibroblasts.

Cells as in (A) were treated or not with thioperamide for 48h or 72h, labelled with filipin (cholesterol) and anti-LBPA antibodies, and analysed by fluorescence microscopy. The panels show the integrated intensity of the filipin (left) and LBPA (right) signals were quantified after 48 (top) and 72h (bottom). The colour code of each fibroblast cell line is as in (A).

26

(C) Quantification of cholesterol in NPC fibroblasts by mass spectrometry.

NPC cell lines (A) were treated or not with thioperamide or 0.1% (2-Hydroxypropyl)-ß-cyclodextrin for 72h. After extraction, lipids were analysed and quantified by mass spectrometry.

(D-F) Quantification of cholesterol in NPC null mice by enzymatic analysis

WT of NPC1 null mice were treated or not with thioperamide for 6 weeks after weaning and sacrificed. The total content of unesterified cholesterol (D) in the corresponding liver extracts was then quantified using an enzymatic assay and is expressed in nmol per mg tissue. The total content of LBPA (E) in the same liver extracts was quantified by mass spectrometry (see Fig EV1), and is therefore expressed as a percentage of total phospholipids. The total LBPA content of WT mice was only marginally increased by the drug, either because the doses were low, or because the contribution from tissue material unaffected by the drug obscured selective changes at the cellular level (despite much effort, we were unable to visualize LBPA in liver samples by immunocytochemistry). The relative ratio of LBPA (E) vs. cholesterol (D) values is shown in (F).

EXPANDED VIEW FIGURE LEGENDS

Figure EV1. (A-B) Electron microscopy analysis of thioperamide-treated cells.

Hela-MZ cells were treated or not with thioperamide, embedded in Epon and processed for electron microscopy (A). Alternatively, cryosections were prepared and labelled with anti-LBPA antibodies followed by 5nm protein A-gold (B); micrographs are same as in Fig 3 (C), but without pseudo-coloring. Bars: (A) 1 µm; (B): 100 nm.

Figure EV2. (A-B) LBPA analysis by mass spectrometry

(A) HILIC liquid chromatography separation of sLBPA, LBPA and PG standards. Extracted ion chromatograms of positive precursor ions at 2ppm mass tolerance of sLBPA (54:3) 1052.8202Da, (42:0) 894.6793Da; LBPA (28:0) 684.4810Da; and PG (28:0)684.4810Da, (28:2) 680.4497Da, (36:2) 792.5749Da

(B) Separation by endogenous LBPA, SLBPA, PG and PS detected in mouse liver extracts (y axis: LC elution time; x axis: m/z of the positive precursor ion. PG: phosphatidylglycerol; LBPA: lysobisphosphatidic acid; sLBPA: semi- lysobisphosphatidic acid; PS: phosphatidylserine.

Figure EV3. (A-B) Analysis of sLBPA in mouse liver.

$Npc1^{-/-}$ and $Npc1^{+/+}$ mice were treated or not with thioperamide, and liver extracts were prepared. All sLBPA species present in the extracts were quantified by LC-MS (as in Fig EV2), and the sum of all species is expressed as a percentage of all phospholipids (A). From the experiments in (A). the total amount of major phospholipid classes in mouse liver are expressed as a percentage of all phospholipids (B). PG: phosphatidylglycerol; LBPA: lysobisphosphatidic acid; PS: phosphatidylserine; PI: phosphatidylinositol; PC: phosphatidylcholine; PE: phosphatidylethanolamine.

Figure EV4. (A-B) Distribution of LBPA and sLBPA species in mouse liver extracts.

The species of LBPA (A) and sLBPA (B) were quantified by LC-MS (as in Fig EV2) in liver extracts of $Npc1^{-/-}$ and $Npc1^{+/+}$ mice, treated or not with thioperamide (as in Fig 6D-F and Fig EV2-3), and are expressed as a percentage of the total. The color code indicates the acyl chain composition of the various species listed in the captions, with the total number of

28

carbon atoms of the 2 (LBPA) or 3 (sLBPA) acyl chains together, and the degree of insaturation. The prefix "e" indicates lipids with one 1-O-alkyl bond; prefix "p" indicates lipids with one 1-O-alkenyl bond. The bottom panels recapitulate the data after grouping lipid species by the number of carbon atoms in 2 (LBPA) or 3 (sLBPA) acyl chains (chain length) or the degree of insaturation n(umber of double bonds).

Figure EV5. (A-B) Distribution of phosphatidylcholine (PC) and phosphatidylethanolamine (PE) species in mouse liver extracts

The experiment and analysis are as in Fig EV4, except that PC (A) and PE (B) species were quantified.

EXPANDED VIEW MOVIE LEGEND

Movie EV1. Principal Component Analysis (PCA)

The data collected in the high content analysis of the screen in A431 cells (Fig 1) were transformed into a set of uncorrelated principal components, with component 1 (X) corresponding to 78% of variance, component 2 (Y) to 9% of variance, and component 3 (Z) to 8 % of variance. The plot is shown in 3D to facilitate the comparison between various conditions. Each point corresponds to the average of replicates, and thecolor code is the same as in Fig 1 (Red = DMSO, Green = U18666A, Light blue = Trimeprazine, Purple = Thioperamide).

EXPANDED VIEW TABLE LEGENDS

Table EV1. Complete dataset of the screen of A431 cells with the Prestwick library

The table contains all the data from the image analysis performed with MetaXpress™. Toxic compounds (more than 40% toxicity) ha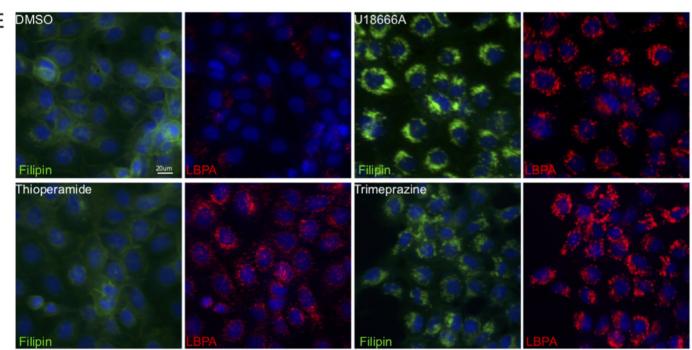ve been excluded from the table. The data are normalized using the Z-score method. Paramet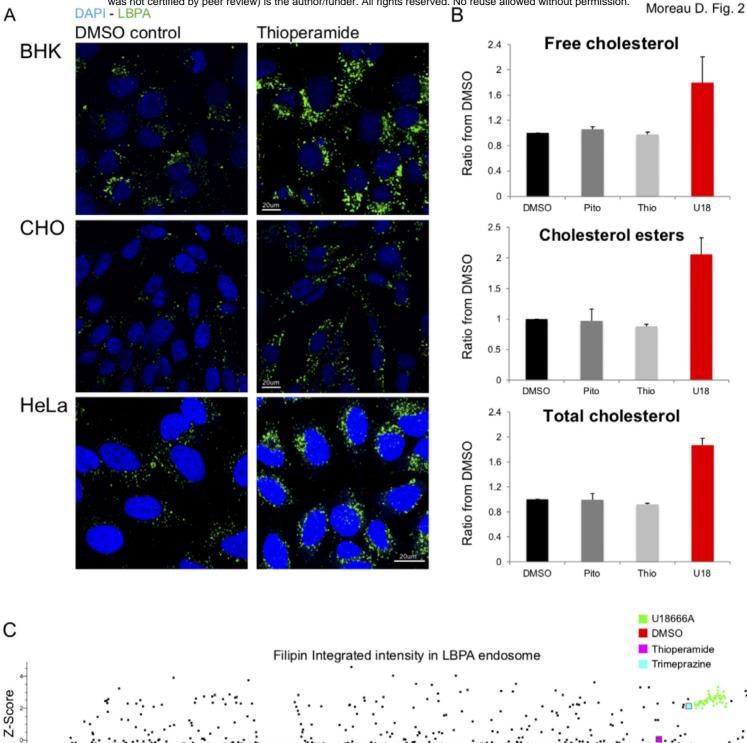ers in each column are expressed using the following nomenclature: Mask name_Channel (on which the mask is applied)_Parameter name.
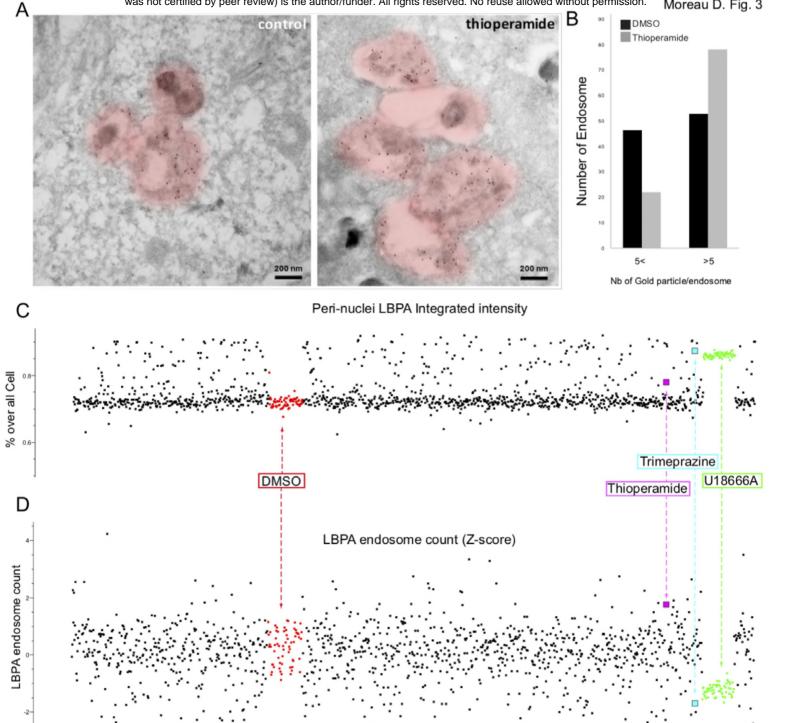
Table EV2. Complete dataset of the screen of HeLa MZ cells with the Prestwick library
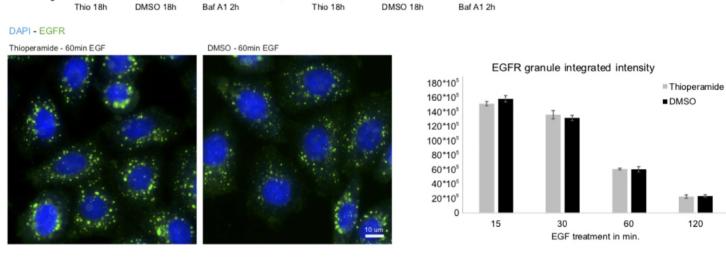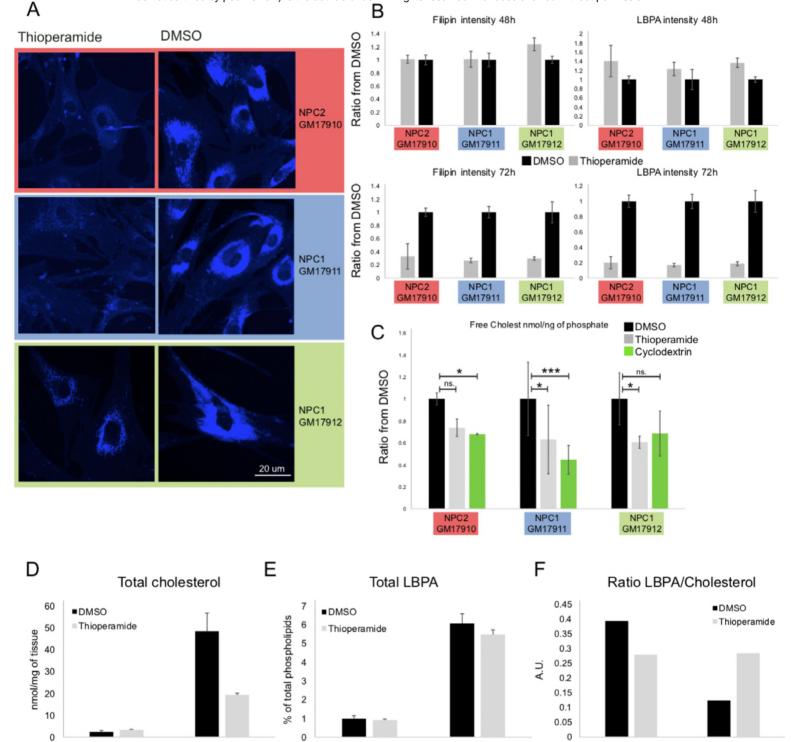
Same as Table EV1 but with HeLa MZ cells.

Moreau D. Fig. 1